Parallel microassembly with a robotic manipulation system

J. Micromech. Microeng. **20** (2010) 125027 (13pp) doi:10.1088/0960-1317/20/12/125027

Parallel microassembly with a robotic manipulation system

Henry K Chu, James K Mills and William L Cleghorn

Department of Mechanical and Industrial Engineering, University of Toronto, 5 King's College Road, Toronto, Ontario M5S 3G8, Canada

E-mail: chu@mie.utoronto.ca, mills@mie.utoronto.ca and cleghrn@mie.utoronto.ca

Received 29 April 2010, in final form 10 October 2010
Published 26 November 2010
Online at stacks.iop.org/JMM/20/125027

Abstract

This paper proposes a methodology to assemble multiple micro-components simultaneously with a robotic manipulator using a parallel assembly method. Through manipulating and assembling the micro-components, intricate, out-of-plane, three-dimensional micro-devices can now be fabricated. Use of a parallel microassembly process rather that a serial approach can significantly increase the productivity and reduce the cost of assembling micro-devices. The parallel microassembly operation proposed in this work was developed and implemented on a 6-DOF robot manipulator to attain considerable manufacturing flexibility. In this study, three passive microgrippers were bonded in parallel to the end-effector of the manipulator. Three microparts were then grasped by the grippers from the worktable of the manipulator, rotated 90°, and assembled onto the base substrate simultaneously. During the parallel microassembly operation, the visual image may not be able to monitor all three gripper-part pairs simultaneously due to the limited field of view of the microscope. Through the use of an alignment-calibration algorithm with only one gripper-part set, the remaining two sets were successfully manipulated and inserted onto the desired assembly location.

(Some figures in this article are in colour only in the electronic version)

1. Introduction

Micro-electromechanical system (MEMS) is an emerging technology applied to the development of sensors and actuators. In general, the term MEMS refers to a micro-sized mechanical structure with integrated electronic components which provides various functionalities. MEMS possesses the advantages of smaller physical size, lower power consumption, lower cost, and higher reliability over many conventional scale systems. The applications of MEMS are multi-disciplinary: MEMS devices can be found in inkjet printer heads and digital mirror displays in the office electronics industry [1], pressure sensors and gyroscopes in the automotive industry [2], and RF switches in the wireless and telecommunication areas [3].

Many micro-fabrication techniques in MEMS originate from the IC industry. These techniques mainly utilize a two-dimensional fabrication process. Three-dimensional structures can only be formed through the deposition of two-dimensional layers onto the substrate. Due to the nature of the process, the design flexibility to fabricate components with three-dimensional features is very limited [4]. To allow for the fabrication of complex three-dimensional micro-devices, the technique of 3D microassembly was introduced.

Microassembly is the process of manipulation and assembly of micro-sized components into MEMS devices. Due to the delicate nature of these micro-sized components, handling and manipulation of these small components for the microassembly processes requires high accuracy and precision to prevent damage and failure during the process. To fabricate complex MEMS devices from essentially flat (2 1/2D) MEMS components, robotic manipulation systems are often used to facilitate the microassembly process. Modern manipulation systems possess multiple degrees of freedom (DOF) and are capable of providing high-precision motion and actuation. For instance, the FC150 bonding system manufactured by Smart Equipment Technology has a total of 6-DOF and the accuracy in translation and rotation is as small as 1 μm and 20 μrad, respectively [5]. Aarts *et al* in [6] have successfully used this system to assemble out-of-plane microprobe arrays. To further increase the manufacturing flexibility of the microassembly process, Popa and his research group [7] developed a 3D microassembly station that can provide a combined 19-DOF

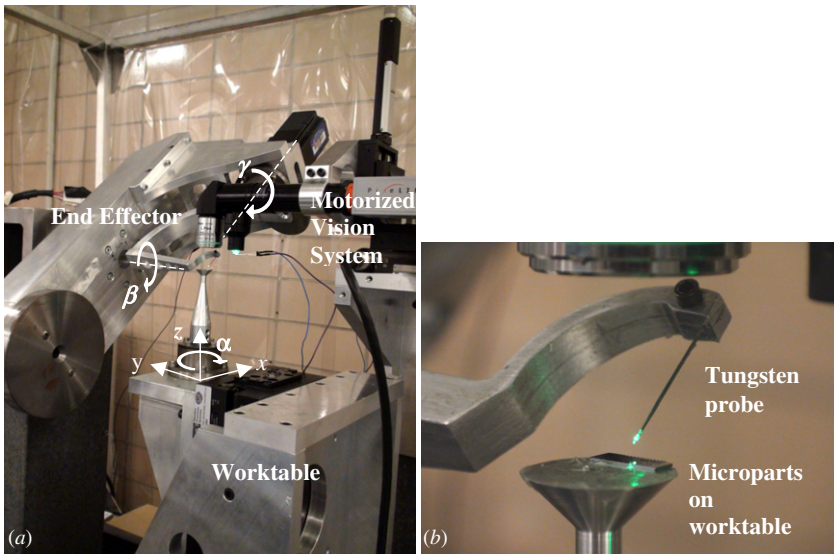

Figure 1. (*a*) The 6-DOF manipulator and (*b*) the magnified view of the MEMS micropart, worktable and tungsten probe.

to the three micromanipulators. Microspectrometer and other MEMS parts were successfully assembled by his research group [7, 8].

Throughout the years, several microassembly processes were proposed and investigated by different research groups. In summary, these processes can be categorized into two types: serial and parallel assembly [9].

In the serial assembly process, micro-devices are assembled at a workstation one device at a time with simple pick-and-place assembly. Tools such as microtweezers and microgrippers are utilized to grasp and assemble the microparts into complete devices. Examples of MEMS devices fabricated through serial assembly include micromirrors [10], electron-beam steering columns [11], and micro crawler robot [12].

In contrast, parallel assembly provides a platform for fabricating multiple micro-devices simultaneously. Hence, parallel assembly has the advantage of higher throughput over serial assembly. To manipulate micro-sized devices simultaneously, Lui *et al* [13] proposed the use of centrifugal force to assemble microstructures simultaneously. In the process, multiple micromirrors were self-lifted off the substrate upward by 90° through the introduction of rotational motion on the platform. Feddema *et al* [14] proposed a method to assemble multiple gear trains through precise wafer alignment. Micro-components were first arranged on separate layers or pallets. After alignment, micro-components on one layer were transferred and assembled onto the other layer through the use of a chemical bath. Meanwhile, Tsui *et al* [15] investigated the use of robotic assembly techniques to manually assemble multiple microstructures in a parallel approach. Parallel sets of microgrippers were installed on a 5-DOF manipulator to assemble an array of microconnectors. As a tradeoff, many of these parallel microassembly operations often have restrictions on the manufacturing flexibility. Many of these operations also require extremely high precision. Hence, research in parallel microassembly operation to date is very limited and is usually task-oriented.

Among the three parallel microassembly methods discussed, the method of robotic parallel assembly possesses the highest degree of manufacturing flexibility. This direct pick-and-place assembly process allows both rotational and translational motions, and hence complex micro-devices can be assembled with this method. In the work presented in this paper, an in-house 6-DOF manipulator was developed and implemented to perform a complex parallel microassembly operation. The additional DOF in this study compared with the 5-DOF system used by Tsui *et al* in [15] allows correction of any orientation mismatch between the parallel microgrippers and the substrate plane, which is crucial to the alignment and assembly processes during parallel microassembly operations.

In many microassembly processes, visual feedback from a top-mounted CCD camera is commonly used to monitor the process. Since the micro-components are very small in size and the assembly process requires high positioning accuracy, a high-magnification objective lens is commonly used to enlarge the viewable image. Under a fixed camera configuration with a high-power magnification lens, the available field of view is typically too small to simultaneously monitor the microassembly process at each gripper. To remedy this limitation, the present study proposed a novel algorithm that requires monitoring of only one gripper in order to perform the entire parallel microassembly operation. Through the alignment strategy in the proposed algorithm, grippers that are outside the field of view can also be aligned and assemble parts onto the target location successfully.

2. Background

2.1. The multi-DOF manipulation system

The 6-DOF manipulator used for the robotic parallel microassembly operation is shown in figure 1. This in-house designed and fabricated manipulator comprises a movable worktable with 4-DOF, and a top structure with 2-DOF, which supports a tungsten probe. The worktable can translate along

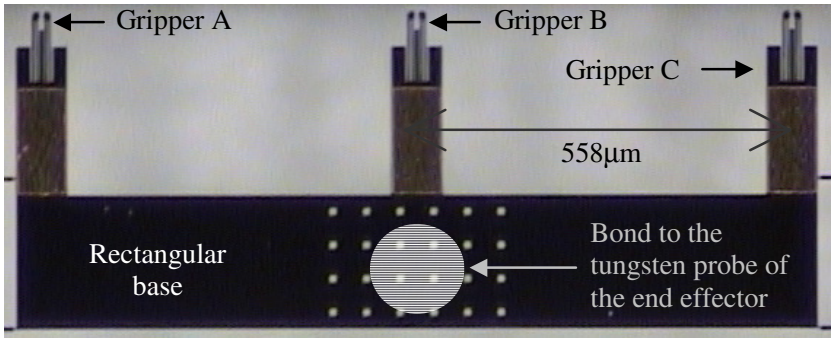

Figure 2. The parallel microgripper layout.

the x-, y-, and z-axes through the translation stages and can also rotate 360° along the α-axis. The top structure allows the tungsten probe to rotate along the β- and γ-axes. The tip of the tungsten probe is located exactly at the intersection between these two axes. Six stepper motors are used to drive the worktable and the tungsten probe on the top structure. These stepper motor drivers are configured so that they can provide a resolution of 0.2 μm per step for translational and 0.072° per step for rotational motions.

To begin the microassembly operation, the microparts to be assembled are placed on the worktable. Manipulation of these microparts is performed with MEMS-based parallel microgrippers. The parallel microgrippers are bonded onto the tungsten probe using Norland Optical Adhesives, NOA63. A thin layer of the adhesive is applied between the probe and the parallel microgrippers and the adhesive is cured using EFPS Ultracure 100SS Plus for 120 s.

A vision monitoring system is installed onto the manipulator to provide visual feedback for the proposed controller. The vision system consists of a monochrome CCD camera with a 20× magnification lens mounted onto a motorized stage on top of the manipulator. The position of the stage may be adjusted either manually or automatically, to acquire a focused image over the entire worktable. The viewable area of the camera is 1024 by 768 pixels, with a pixel pitch of 0.33 μm. The combined vision system provides a field of view of 387 by 290 μm. Details of the manipulation system are discussed in [16, 17].

2.2. Fabrication of micro-components

Microparts and microgrippers used in the experiments were fabricated with the SOIMUMPs micromachining process [18]. The silicon-on-insulator (SOI) wafer used comprises a 25 μm silicon top layer, a 400 μm silicon substrate, and a 1 μm oxide as the insulating layer in between. The silicon top layer was fabricated into the structures of micro-components, while the substrate was used for handling purposes.

2.3. Microgripper design

The proposed parallel microassembly operation requires multiple microgrippers to be installed onto the end-effector of the manipulator. In this work, three microgrippers in a parallel configuration are proposed to grasp and assemble

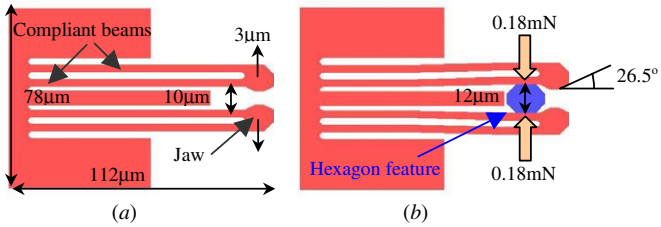

Figure 3. Schematic of the microgripper design (a) before grasping and (b) after grasping.

three microparts simultaneously. Figure 2 shows the layout of the three parallel microgrippers. Each microgripper has dimensions of 112 by 78 μm and is 558 μm apart from the adjacent microgripper(s). In order to bond these grippers onto the end-effector of the manipulator, each gripper is connected to a common rectangular base, where the center of the rectangular base is bonded to the end-effector of the manipulator.

To minimize the size of the parallel microgrippers' structure, a passive, snap-locking design [19] was employed to operate the grasping actions of the microgripper. With the passive actuation mechanism, the microgrippers will not require microactuators such as shape-memory alloys, electrostatic, piezoelectric or thermal actuators [20]. The grasping motion of the passive gripper jaws used in the proposed parallel assembly process is directly dependent on the elastic deformation of the compliant beams of the microgrippers, as shown in figure 3. As a gripper grasps the micropart, the assembly force exerted on the microgripper jaws will force the compliance beams to deform and open the jaws. The modeling equation between the assembly force and the opening is given by Prasad *et al* [21] as

$$F = k\Delta\frac{\mu + \tan\phi}{1 - \mu\tan\phi} \tag{1}$$

where $\boldsymbol{F}$ is the assembly force, $\boldsymbol{k}$ is the stiffness of the gripper, $\boldsymbol{\Delta}$ is the width of the jaw opening, $\boldsymbol{\mu}$ is the friction coefficient, ϕ is the inclined angle between the force and contact surface.

Equation (1) was used to evaluate the required assembly force in this work. The proposed gripper is required to open 6 μm in order to fully grasp the hexagon feature of the micropart. The stiffness of the grippers is contributed from the two 2 μm compliant beams with a length of 98 μm on

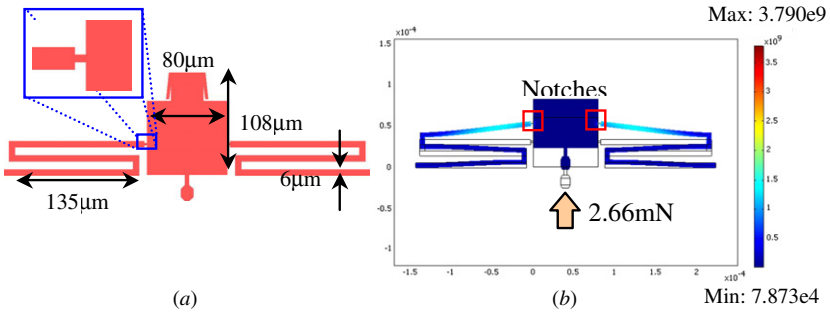

Figure 4. (*a*) Schematic; (*b*) finite element result of the micropart.

each jaw. Using the model of a guided cantilever beam, the lateral stiffness was evaluated to be 188 N m^{-1}. The inclined angles at contact surfaces, for both grasping and releasing of an object, were designed to be 26.5°, as shown in figure 3(*b*). For a 3 μm displacement on each jaw, the assembly force was evaluated to be 1 mN, using a friction coefficient of 0.3 [22].

In order to grasp the micropart firmly during the manipulation process, the gripper jaws will not close completely after the 3 μm opening. Once the hexagon feature of the micropart reaches the locking position as shown in figure 3(*b*), the gripper jaws retract back only 2 μm, and the compliant beams are still deformed by 1 μm. Using the lateral stiffness, as calculated earlier, this 1 μm deformation can provide a total of 0.36 mN clamping force to hold the object.

2.4. Micropart and supporting tether design

Microparts with dimensions of 108 μm by 80 μm were fabricated for the parallel assembly process [23]. To facilitate passive grasping, the design of microparts incorporated a hexagonal feature for snap-locking with the microgripper jaws. The hexagonal feature has a symmetric shape so that it can ensure that the force required to open the jaws on the left and right is equal and the opening/releasing force are the same. The micropart was suspended through two tethers as shown in figure 4. The dimensions of tethers of the micropart were designed so that the force required to break tether was higher than that to open the gripper jaws. Result of a finite element analysis shows that an insertion force of 2.66 mN is needed in order to approach the yield stress limit of the tethers at a stress of 3790 MPa [24] at the 2 μm wide notches, as shown in figure 4(*b*).

2.5. Mechanical joint design

The microassembly operation proposed involves rotating the micropart 90° to the plane of the substrate and assembling the micropart perpendicularly onto the base substrate [25]. The mechanical joint between the micropart and the base substrate must be designed properly to facilitate the assembly. An insert-and-lock feature with two flexible legs and a rectangular slot were implemented on the micropart and the base substrate, respectively. The perimeter of the rectangular slot was designed such that it allows the micropart to be inserted easily. The two flexible legs on the micropart will lock the part in place after the part has been completely inserted into the slot. Details of the mechanical joint design are shown in figure 5.

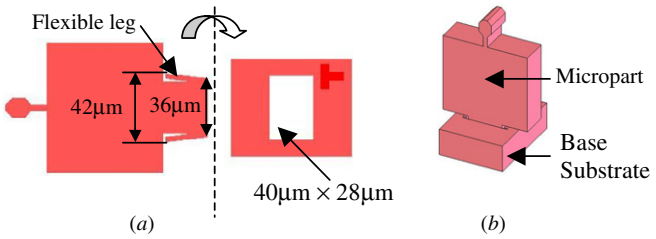

Figure 5. (*a*) Schematic of the mechanical joint; (*b*) micropart assembled on the base substrate.

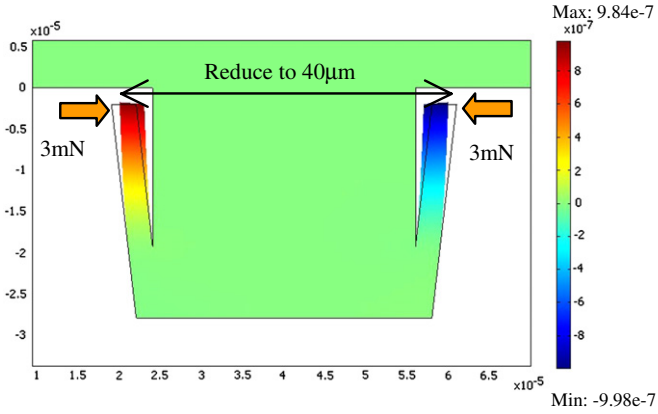

Figure 6. Displacement of the two flexible legs under 3 mN load on each side.

It was determined that a force of 3mN is required on each side to bend the two legs by 1 μm, as shown in figure 6. Using 0.3 as the friction coefficient for SOIMUMPs, the static frictional force, which is the minimum force required to extract the micropart after being inserted into the rectangular slot, is computed to be 1.8 mN. From the previous section, a force of 1.44 mN is required for the passive gripper to release the part from its jaws. Since a larger force is required to extract the micropart from the slot, the gripper can release the part after the 90° insertion.

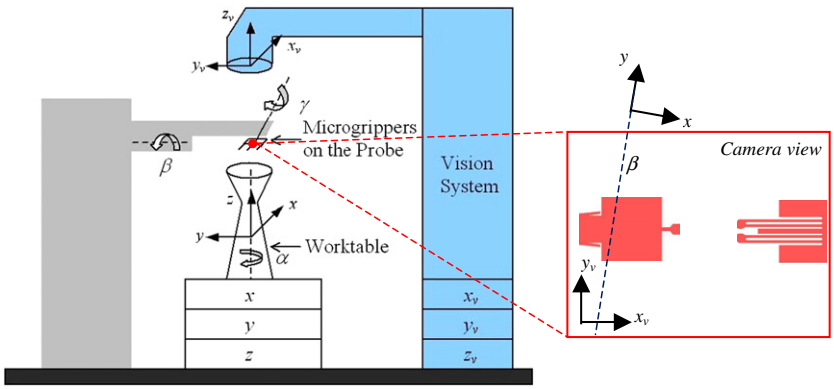

Figure 7. Schematic drawing of the manipulation system.

2.6. Parallel strategy

In many serial microassembly processes, the entire process is monitored through CCD cameras to assist in part manipulation. A high-magnification objective lens is often used to provide more details of the microgripper and the micropart in the assembly process. When using a similar visual system configuration for the parallel assembly, the field of view of the camera will then become insufficient to capture all gripper-part sets. Changing the objective lens with a lower magnification to increase the viewable area is not recommended as it will lead to a loss in resolution in the operation. Multiple cameras or a movable camera with long travel range may solve the problem, but it will increase the cost and complexity of the process. In this work, a single CCD with short travel range was used to perform the parallel microassembly. The CCD camera was used to monitor the microassembly process on only one gripper-part set. High-precision alignment-calibration strategy is employed so that the microgripper part located outside the field of view can also be assembled properly without the need of visual supervision. Details of the strategy are discussed in section 3.

2.7. System model

As discussed in section 2.1, the manipulator can provide a total of 6-DOF for the microassembly operation: 4-DOF for the microparts on the worktable and 2-DOF for the microgrippers on the probe. The positioning stage of the vision system itself provides 3-DOF to the CCD camera. Figure 7 shows the schematic view of the system. During the operation, the x_v- and y_v-axes of the vision system frame remain at the same position after searching and locating the probe under the magnified image. The z_v-axis, on the other hand, is used primarily for image focusing and height evaluation purposes. When setting up and calibrating the manipulation system, the system is originally configured so that the robot frame (x, y, z) is roughly aligned with the vision system frame (x_v, y_v, z_v). The β-axis of the manipulator, which is used to rotate the microparts by 90° for the parallel insertion operation, is roughly aligned with the y-axis of the robot frame. Nevertheless, slight misalignment could exist between the β-axis and the vision system frame, and this misalignment would result significant height deviation in the parallel insertion operation. In order to achieve high precision in micro-manipulation, a β-axis correction strategy, discussed in section 3.3, was employed to compensate the misalignment.

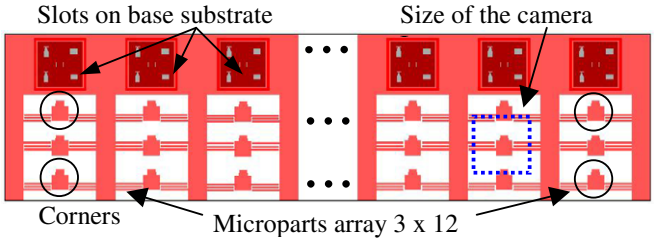

Figure 8. Schematic drawing of the MEMS chip (not to scale).

In this work, microparts were fabricated on a MEMS chip in a 3 by 12 array, as illustrated in figure 8. After loading MEMS chip on the worktable, images of the micropart at the four corners of the chip were inspected under the microscope through the x- and y-axes manipulation of the robot worktable. This visual inspection can check whether or not the x–y plane of the robot frame is co-planar with the x_v–y_v vision plane. Because of the limited depth of field of the system, the micropart image will appear as a sharp image only if the micropart lies approximately on the focus length of the system. If a blurred or out-of-focus image was observed at any of the four corners, the two planes are misaligned. In this work, the vision system acquired a focused image from all the four corners; hence, the x–y plane and the x_v–y_v plane are relatively co-planar.

The alignment strategy and the insertion operation conducted in this work are developed using a vision-based measurement technique. To facilitate the parallel microassembly operation, the microgrippers and the microparts are positioned and aligned with the vision frame as depicted in figure 7.

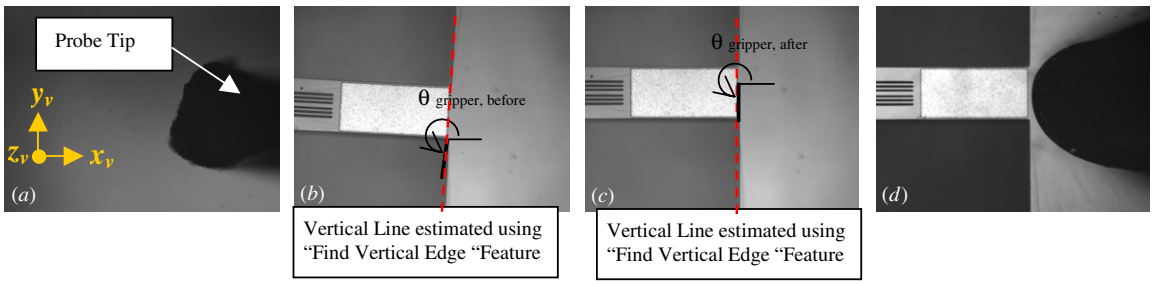

Figure 9. Image from the vision system: (*a*) the tungsten probe tip; (*b*) the microgrippers at the original position; (*c*) the microgrippers at proper orientation and (*d*) the microgrippers bonded onto the probe.

3. Process flow of parallel microassembly operation

3.1. Bonding process of the parallel microgripper

Prior to the parallel microassembly operation, the parallel microgrippers must be bonded onto the tungsten probe of the manipulator. The MEMS chip, with the parallel microgrippers, was placed on the platform of the movable worktable, and the bonding process was performed with the assistance of the visual monitoring system. The visual system was first positioned to focus on the tip of the tungsten probe, as shown in figure 9(*a*). To provide a safe distance for the microgrippers' alignment, the visual monitoring system was then displaced in the negative z_v-direction to move the focal plane 300 μm underneath of the tungsten probe. The worktable was manipulated using the coarse-to-fine approach to find the parallel microgrippers. The light intensity of the visual image background was monitored as the indicator to correct the step size of the increment. Initially, the worktable was manipulated in increments of 100 μm, and the increment was gradually reduced to 0.2 μm as the background changed from dark to bright. The manipulation was stopped when the parallel microgrippers appeared in focus on the visual system. The technique of auto-focusing through contrast measurement was employed to determine whether or not the parallel microgrippers are in focus. When the microgrippers are in focus, the contrast in the image will be the highest as compared to a blurred image. At that position, the normalized focus value, which is the standard deviation over the mean, will reach the maximum value [26, 27]. The initial orientation of the parallel microgrippers, as shown in figure 9(*b*), may not align with the camera frame. This angular misalignment can be evaluated using the 'Find Vertical Edge' feature in LabVIEW [28], and the correction can be performed through the α-axis rotation of the worktable. To correct the orientation of the microgrippers, $\theta_{\text{gripper,before}}$ as depicted in figure 9(*b*), was evaluated. This deviated angle was used to compute the required α rotational input to the worktable, with an angular step resolution of 0.072°. The microgrippers were rotated to the proper orientation as shown in figure 9(*c*). After the orientation adjustment, the visual system actuated 300 μm in the positive z_v-direction and focused back onto tungsten probe. A small amount of UV adhesive was applied on the tips of the tungsten probe. The worktable was then moved upward in the z-direction which brought the parallel microgrippers in contact with tungsten probe. A UV lamp was used to solidify the adhesive between the parallel microgrippers and the tungsten probe and bonded them together, as shown in figure 9(*d*).

3.2. Localization and re-orientation of the micropart for grasping

In this operation, the passive parallel microgrippers must remove three microparts from the MEMS chip simultaneously and assemble them 90° perpendicular to the base substrate. Initially, the vision monitoring system is configured so that the middle gripper (Gripper B) of the parallel microgrippers, shown in figure 10(*a*), is in focus. The microparts, with arbitrary orientation, are then positioned on the platform of the movable worktable. The translational and rotational axes of the worktable are then used to control the position and orientation of the micropart. During the microassembly, the worktable platform advances in the z-direction until a micropart is located within the viewable area of the vision system. A distance of about 300 μm in the z-direction is maintained between the microgrippers and the microparts to avoid collision during the orientation adjustment process. Due to the height difference, the micropart on the left-half plane of the image is out of focus, as shown in figure 10(*b*).

Using visual measurement techniques, the actual height deviation between the microgripper and the micropart can be evaluated explicitly [17]. The motorized stage of the vision system is actuated at incremental steps of 1 μm in the z direction until the micropart on the left-half plane is in focus, as illustrated in figure 10(*c*). The technique of auto-focusing, as discussed in the previous section, was employed to determine whether or not the micropart is in focus. The light intensity in the left-half plane is monitored during each incremental step, and used to compute the normalized focus value. The motion of the vision system stage does not advance further when the normalized focus value starts to decrease. The distance which the vision system traveled in the z-direction until the image is in focus is recorded and used to move the microparts to the same z-coordinate value with the microgrippers in subsequent processes. Figure 11 shows the change in the normalized focus value on the left-half plane between figures 10(*b*) and (*c*).

As the worktable turns during the orientation process, the micropart may be turned away from the field of view of the camera due to off-center rotation, as shown in figure 12. To remedy this situation, the additional displacement applied onto the micropart due to off-center rotation is evaluated.

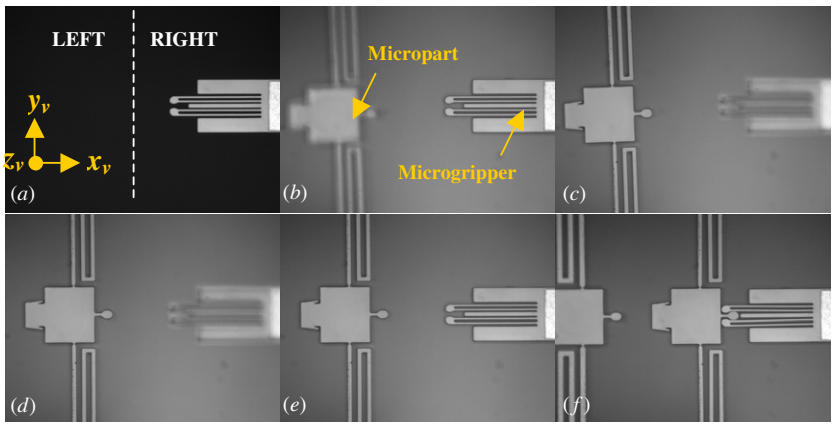

Figure 10. Image from the vision system: (*a*) with the left and right plane; (*b*) when the right-half plane is in focus; (*c*) when the left-half plane is in focus; (*d*) micropart rotates to the proper orientation for grasping; (*e*) microgripper at the same z-coordinate value for grasping and (*f*) microgripper successfully grasps the micropart.

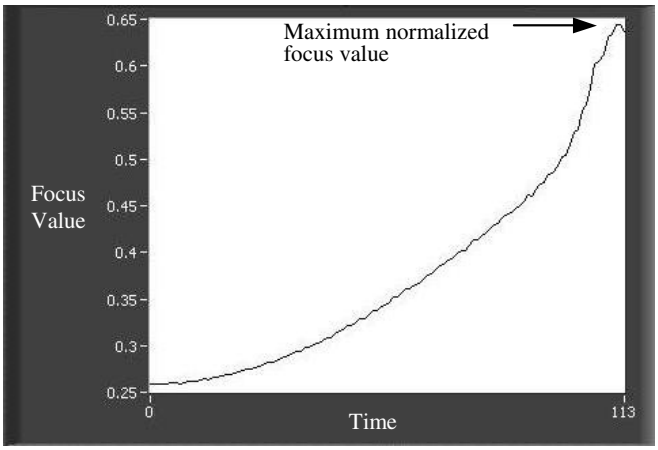

Figure 11. Normalized focus value as the micropart becomes focused.

The discrepancy between the two positions is then utilized to compute the displacement input required to re-position the micropart. Through simultaneous corrective translational motions from the worktable, the micropart could be maintained at its initial coordinates during the process, as shown in figure 10(*d*) [29].

After the microparts rotate to the proper orientation, the microparts are brought to the same z-coordinate height as the microgrippers. The motorized stage of the CCD camera will then re-adjust its position to focus the image on both microgripper and micropart for assembly, as illustrated in figure 10(*e*).

To detach the microparts that are suspended above the substrate through tethers, the worktable first advances the microparts forward and engages them with the passive microgrippers, as shown in figure 10(*f*). After the microgrippers grasp the microparts, the worktable then continues to advance forward to break all the supporting tethers. Once the microparts are detached, the microparts on each gripper can be inspected through the vision system. In the case that the microparts do not orient properly, the parallel grasping and detachment process will be repeated.

3.3. β-axis correction before the 90° rotation

The next step in the microassembly operation is to rotate the microgrippers with the grasped microparts 90° along the rotation axis, β, for the vertical insertion process. To ensure successful simultaneous insertion of the microparts, each micropart must be positioned at the same z-coordinate above the base substrate, after the β-axis rotation. When bonding

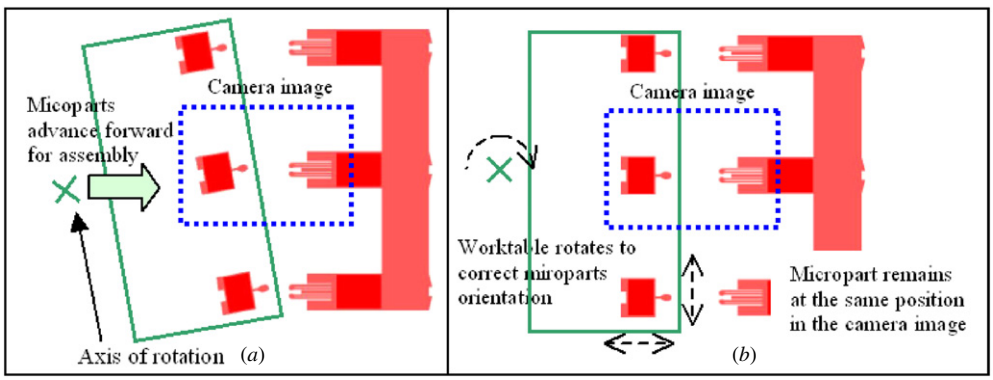

Figure 12. Image of the grippers and microparts (*a*) before α-rotation and (*b*) after α-rotation with displacement compensation.

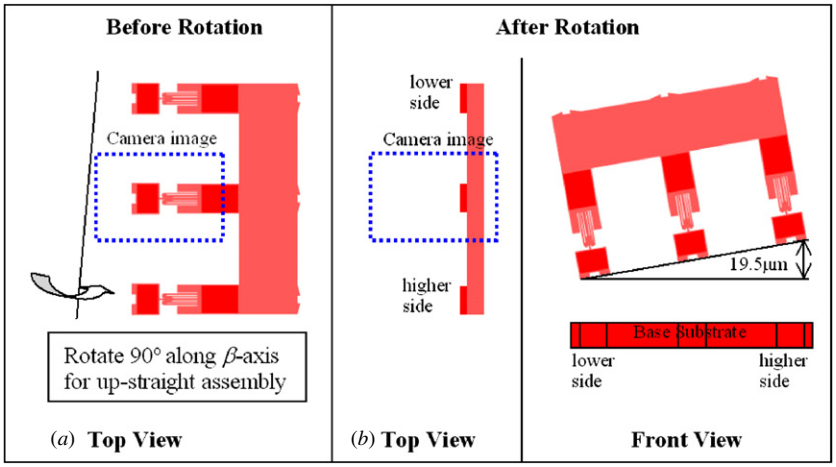

Figure 13. Error due to misalignment between the β-axis and the vision system frame: (a) before and (b) after 90° rotation.

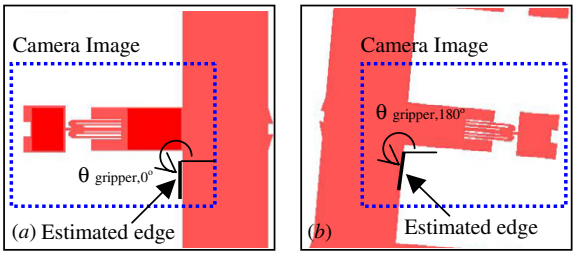

Figure 14. Microgripper at (a) 0° and (b) 180°.

the microgrippers onto the probe of the manipulator, the microgrippers are aligned with the vision frame initially. As discussed in section 2.7, slight misalignment between the β-axis and the vision system frame in the system could exist and this will lead to a z-coordinate height deviation between the microparts after the β-axis 90° rotation. In this work, each gripper is 558 μm apart and a 1° misalignment will result in a height deviation as large as 19.5 μm over the span of the parallel microparts, as shown in figure 13.

To eliminate this z-coordinate height deviation, the orientation of the microgrippers must be adjusted and aligned with the β-axis, prior to the 90° β-axis rotation. The actual angular deviation, between the β-axis and the vision system frame, was evaluated through an experimental approach. Prior to the β-axis rotation, the orientation of the microgrippers at 0° β ($\theta_{\text{gripper},0^o}$) was measured. Using the 'Find Vertical Edge' feature of LabVIEW, the edge of the microgrippers in the visual image, illustrated in figure 14, was estimated and this edge was used to represent the orientation of the microgrippers. The value of $\theta_{\text{gripper},0^o}$ is measured from the angle inscribed by the vertical edge of the microgrippers and the x_v-axis, prior to the β-axis rotation. As discussed in section 2.7, the microgrippers were pre-aligned with the x_v-axis of the visual system. Hence, $\theta_{\text{gripper},0^o}$ should have a value of approximately 270°. At a later stage, the β-axis was commanded to rotate 180°. At this new orientation, the angle between the vertical edge of the microgrippers and the x_v-axis was measured again. This new angle, $\theta_{\text{gripper},180^o}$, together with $\theta_{\text{gripper},0^o}$ was then used to evaluate the angle of the β-axis (θ_{beta}) with respect to the x_v-axis of the vision frame:

$$\theta_{\text{beta}} = \theta_{\text{gripper},0^o} - \frac{\theta_{\text{gripper},0^o} - \theta_{\text{gripper},180^o}}{2} \tag{2}$$

where θ_{beta} is the angle of the β-axis with respect to the vision frame, $\theta_{\text{gripper},0^o}$ is the orientation of the gripper in the visual image at 0°, $\theta_{\text{gripper},180^o}$ is the orientation of the gripper in the visual image after 180° rotation on the β-axis.

This work proposed an approach which utilizes the γ-axis of the manipulator and the images from the top-view camera in order to correct the height deviation between each micropart. Schematic of the correction process via the γ-axis approach is depicted in figure 15. The γ-axis, concentric with the tungsten probe, can provide 360° rotational motion along the tungsten probe. This approach eliminates the need of either re-calibrating the entire system or re-bonding of new parallel microgrippers to compensate the angular deviation between the β-axis and the y_z-axis of the vision system. When the microgrippers were bonded onto the tungsten probe, the tungsten probe, as well as the γ-axis, forms a 45° angle to the surface of the microgrippers, as shown in figure 15(a). Hence, rotating the microgrippers about the γ-axis will provide coupled rotational motions equivalent to rotating the microgrippers concurrently along both the z_v- and x_v-axes shown as the two circular arrows in figure 15(a). With aid of the top-view image, the microgrippers were monitored and were gradually rotated about the γ-axis until the orientation of the microgrippers, θ, is equal to the evaluated θ_{beta} from the top view as illustrated in figures 16(c) and 17(c). As discussed, the rotation of γ-axis will also generate a coupled rotational motion along the x_v-axis, and the microgripper will be tilted with respect to the vision x_v-y_v frame, as demonstrated in figures 16(b) and 17(b). However, this undesired rotation along the x_v-axis would not affect the height of each micropart. When the orientation of the microgrippers, θ, aligns with θ_{beta}, the distance between each micropart and the β-axis becomes the same. Hence, after the β-axis 90° rotation in the later step, microparts will not experience the height deviation problem as shown in figure 17(d). The undesired rotation along the x_v-axis would

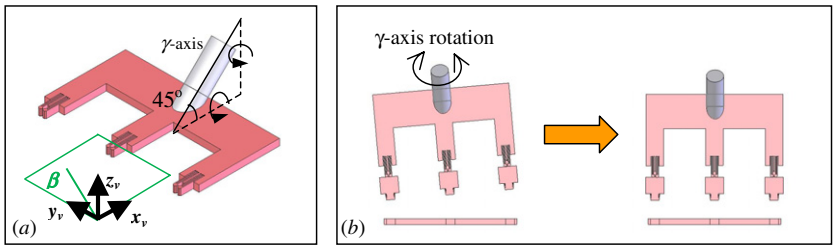

Figure 15. Schematic to show (*a*) the coupled rotational motion due to γ-axis rotation and (*b*) γ-axis rotation to correct the height deviation between each micropart.

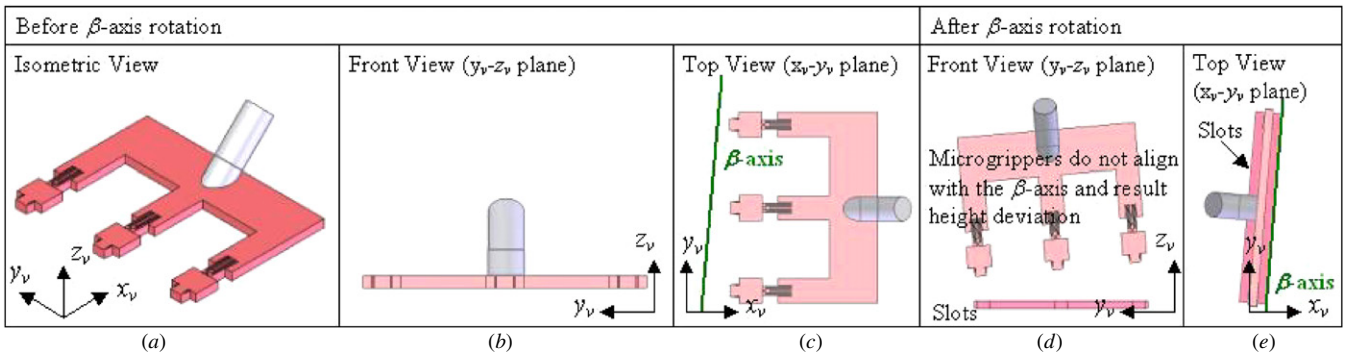

Figure 16. Different camera views without the γ-axis correction: (*a*) isometric view; (*b*) front view; (*c*) top view of the microgrippers; (*d*) front view and (*e*) top view of the microgrippers after β-axis 90° rotation.

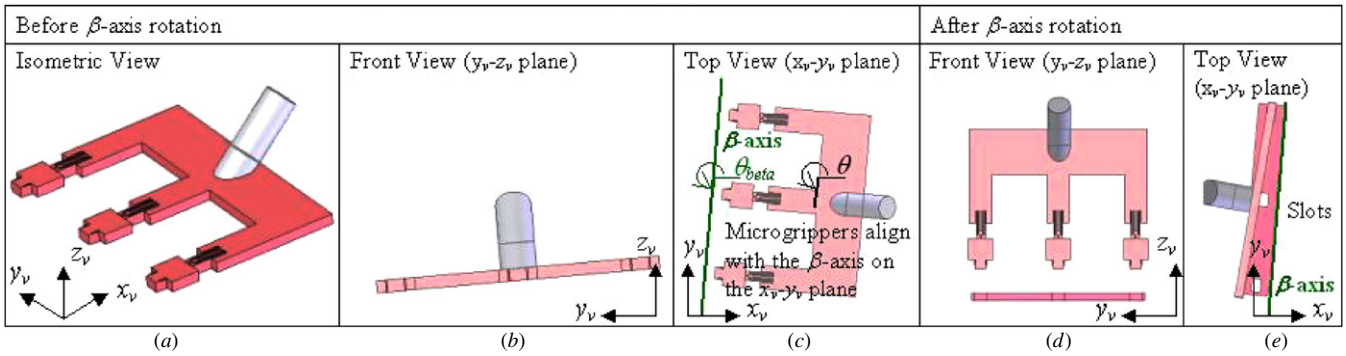

Figure 17. Different camera views with the γ-axis correction: (*a*) isometric view; (*b*) front view; (*c*) top view of the microgrippers; (*d*) front view; (*e*) top view of the microgrippers after β-axis 90° rotation.

only introduce an addition offset or rotation along the z_v-axis after the β-axis 90° rotation, as illustrated in the top view in figures 16(*e*) and 17(*e*). This offset can be compensated easily by turning the base substrate at the insertion step as described in the following section.

3.4. Alignment strategy between the micropart and the base substrate for 90° insertion

After completing the β-axis correction process as discussed in the previous section, the microparts are rotated 90° to the vertical insertion position. The in-house 6-DOF manipulator is configured so that the microparts will still be maintained at the same position in the camera view after rotated 90° along the β-axis. The motorized stage of the vision system in the z-direction was actuated to achieve an image focused on the insertion tip of the micropart, as shown in figure 18(*b*). Based on the image, the edge on the insertion tip is projected for use in the latter alignment process.

Since both the microparts and the base substrate are manufactured on the same chip, the lateral distance between the microparts and the base substrate is known. Using this information, the worktable manipulates and positions the slot on the base substrate within the microscope view. To precisely align the micropart with the slot for the insertion operation, the visual alignment technique is implemented in two stages to align the orientation and position the base substrate with respect to the micropart. In the first stage, the motorized stage of the vision system actuates backward in the z-direction so that the rear side of the parallel microgrippers is in focus. The rear side of this 25 μm thick gripper on the image will appear as a line 25 μm wide as shown in figure 18(*c*). From the image, the orientation of the microgrippers after the 90° rotation, with respect to the vision frame, can be evaluated.

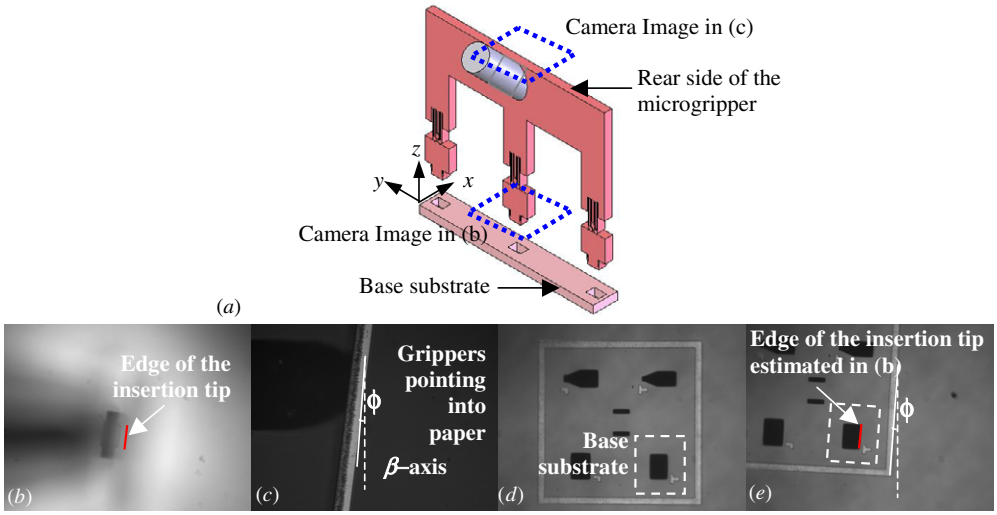

Figure 18. (*a*) Isometric view showing the microgripper after 90° rotation; (*b*) camera focused on the edge of the gripper; (*c*) camera focused on the tip of the micropart at 90°; (*d*) camera zoomed to the substrate to the evaluated the angle and (*e*) the substrate rotated to the evaluated angle.

Without the γ-axis rotation, the rear side of the gripper should be parallel to the β-axis ($\phi = 0$). However, after the γ-axis adjustment, the rear side of the gripper will possess an angular offset ($\phi > 0$) with respect to the β-axis. Through the use of the 'Find Vertical Edge' feature to compute the orientation of the microgrippers, the angle ϕ can be calculated. To complete the assembly operation, the base substrate must be positioned underneath the micropart. In the second stage, the motorized stage of the vision system actuates forward in the z-direction and brings the base substrate in focus, as shown in figure 18(*d*). Prior to the assembly, the base substrate needs to be rotated to the same orientation as the micropart. In addition, the slot of the base substrate must be moved laterally so that the edge of the micropart insertion tip estimated previously should fit in the base substrate, as illustrated in figure 18(*e*). As a result, the base substrate is in the proper position ready for the insertion operation.

3.5. Micropart assembly and gripper removal

The last operation in the microassembly process is to insert the microparts onto the base substrate and then release them. After the alignment process, the vision system is positioned to focus on the insertion tip of the micropart. The worktable is then commanded to rise in the positive z-axis direction for the insertion operation. As the worktable rises, the base substrate becomes visible from the screen. The actual insertion begins when the image of the base substrate gradually comes in focus. In order to lock the micropart into the base substrate, the micropart tip needs to be inserted into the base substrate at a distance of 20 μm. In this work, the worktable is commanded to rise slowly for 25 μm in increments of 1 μm. The extra 5 μm movement is to ensure that the microparts are completely inserted into the base substrate. After the three microparts are inserted into the slot on the base substrate, the parallel microgrippers release the parts. Depending on the operation, the microparts can be released by moving the parallel microgrippers either vertically or laterally, as depicted in figures 19(*b*) and (*c*). The vertical releasing scheme is the most direct approach to release the microparts in a compact environment. This scheme requires the holding force generated from two flexible legs to be sufficient to hold the microparts in place during the releasing, as discussed in section 2.5. On the other hand, the lateral releasing scheme does not solely rely on two flexible legs to provide the holding force. The entire micropart tip will provide the holding force as the microparts slide aside from the grippers.

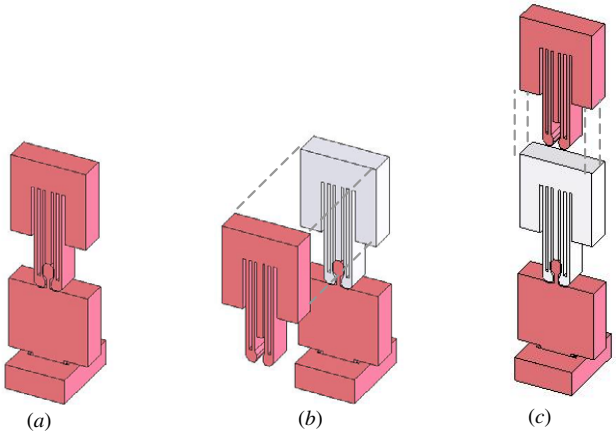

Figure 19. (*a*) Micropart was inserted onto the substrate; (*b*) micropart was released laterally and (*c*) vertically.

4. Experiment and discussion

The proposed parallel microassembly strategy as outlined in section 3 was examined experimentally through an in-house 6-DOF manipulator as described in section 2.1. The parallel microgrippers on the probe of the manipulator were

Table 1. Experimental results from the two releasing schemes.

	Vertical releasing scheme			Lateral releasing scheme		
Trial	No of microparts inserted	No of microparts remained in the slot	Success rate	No of microparts inserted	No of microparts remained in the slot	Success rate
No 1	2	1	50%	1	1	100%
No 2	1	0	0%	3	2	67%
No 3	3	2	67%	1	0	0%
No 4	3	1	33%	3	3	100%
No 5	1	0	0%	3	3	100%
Average	10	4	40%	11	9	82%

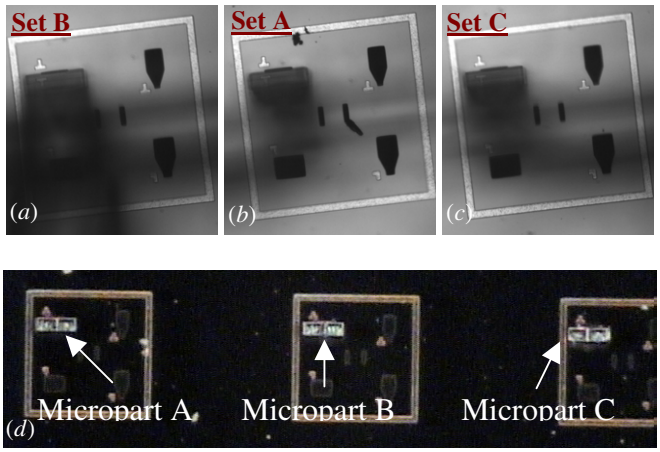

Figure 20. Top view of the (*a*) micropart B; (*b*) micropart A; (*c*) micropart C after insertion, at 1× magnification; and (*d*) top view of the micropart after release, at 20× magnification

manipulated to detach and assemble three microparts at a 90° angle with respect to the substrate. Figure 20(*a*) shows the camera view at the instant the micropart is inserted and locked onto the substrate. The insertion processes at the other two grippers are included in figures 20(*b*) and (*c*) for illustration purposes only as the proposed strategy only requires visual feedback on one gripper. After the three microparts are locked onto the substrate, the three microgrippers are retracted to release the microparts. Figure 20(*d*) shows the picture of three microparts using a low-magnification microscope. Both micropart releasing schemes described in section 3.5 were tested experimentally in this study. For the scheme to retract the microgripper in the vertical direction, away from the substrate, it was observed that many of the microparts were pulled out from the base substrate during the process. Out of the ten successfully inserted microparts, only four microparts (or 40%) remain in the slot. The pull-out failure is suspected to be the result of insufficient force provided by the mechanical joints to hold the microparts in place after the insertion. In contrast, experimental results show that retracting the microgripper laterally yielded a success rate of over 80% (9 out of 11). Table 1 summarized the experimental results conducted to investigate the effectiveness of the two micropart releasing schemes from five trials.

During the lateral releasing scheme, because the slots on the substrate have a slight larger geometry than the legs, there exists possibility that the microparts might be tilted at an angle with respect to the surface of the substrate. Figure 21(*a*) shows an exaggerated view of the tilt. Based on the geometry of the microparts and the slots, a tilt angle as high as 12° could result as the parts were released laterally if there were no friction force between the slot surface and the inserted portion of the part. However, depending on the value of this fiction force, part stiffness, and the depth of insertion, the micropart may be able to resist against tilting during the part releasing motion. Through visual inspection on the assembled parts, it was observed that the microparts were not notably tilted after releasing the parts using the lateral releasing scheme.

When inspecting the microparts under the microscope, discrepancies between the design and the fabricated micropart flexible legs were observed. In the original design, the two flexible legs were constructed by etching away two 2 μm by

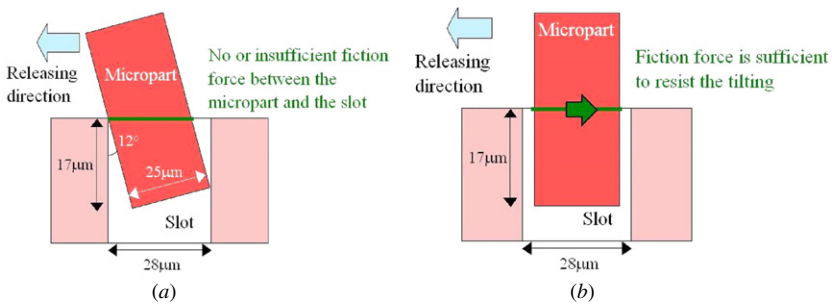

Figure 21. Schematic showing (*a*) the maximum possible tilting during the lateral releasing scheme, with insufficient or no fiction force and (*b*) with sufficient friction force.

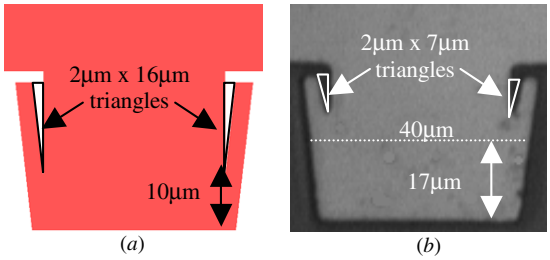

Figure 22. Flexible legs on the (*a*) schematic drawing and (*b*) fabricated micropart under the microscope.

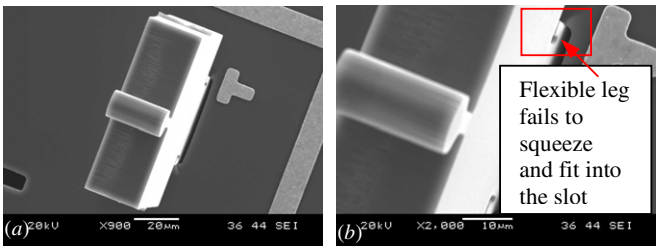

Figure 23. SEM image of the micropart under (*a*) 900× and (*b*) 2000× magnification.

16 μm triangles from the microparts, as shown in figure 22(*a*). The etching area was specially designed to allow the squeezing action to initiate at an insertion distance of 10 μm. However, it was observed from the fabricated microparts that triangles of only 2 μm by 7 μm were etched away from the microparts, as shown in figure 22(*b*). The discrepancies caused the two flexible legs to be shorter than anticipated. It was determined that the squeezing action would not take place until an insertion distance of 19 μm was achieved. As observed from the geometry of the fabricated microparts in figure 22(*b*), a significant portion of the micropart tip is larger than the 40 μm wide rectangular slots on the base substrate. Hence, the microparts might not be fully inserted into the slots, as illustrated in figure 23. Hence, the flexible legs would not be able to lock the microparts in place. Instead of the retracting force from the two flexible legs, only friction force would be present to hold the microparts in place during the microgripper retracting process. As a result, releasing the microparts through retracting the gripper vertically a high failure rate was experienced during the experiments.

Another factor that influences the success rate of the parallel microassembly experiments is the orientation error introduced on the microparts during the tether breaking process. After the parallel microgrippers grasp the microparts, they continue to advance forward in order to break the supporting tethers. In this study, the grippers were designed to secure the microparts firmly during the microassembly operation through the force arising from the compliant beams on the grippers, as evaluated in section 2.3. During the experiment, it was observed that the micropart could be shifted vertically or horizontally away from the desired orientation, as illustrated in figure 24, during the tether breaking process.

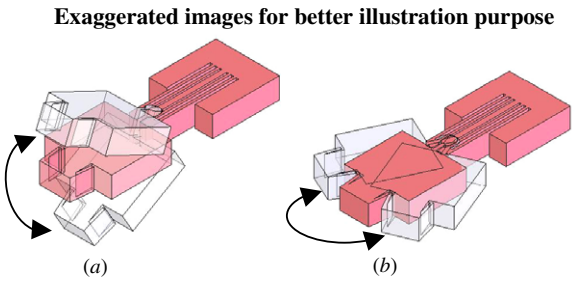

Figure 24. Micropart shifted (*a*) vertically and (*b*) horizontally; during the tether breaking process.

5. Conclusion and future work

A parallel microassembly process was developed to allow the assembly of multiple micro-components simultaneously. The parallel microassembly operation was developed on the basis of robotic micromanipulation processes. In the present work, the process was implemented on a 6-DOF robotic manipulator. Sets of three microparts were grasped by the parallel microgrippers from the worktable of the manipulator, rotated 90°, and assembled onto the base substrate. During the assembly operation, the limited field of view of the microscope was not large enough to monitor all three gripper-part sets. To overcome this limitation, the alignment and calibration algorithm proposed in this work only required monitoring one gripper-part set. The remaining gripper-part sets were successfully manipulated and assembled. Experiments confirmed that the three microparts were successfully grasped and assembled onto the target base substrates. In addition, it is observed that a higher success rate of releasing the parts can be achieved through retracting the microgripper laterally instead of vertically.

The success rate of the parallel microassembly operation experimented in this study may be improved with some modifications on the designs of the parallel microgrippers and the microparts. When fabricating the microparts, it was observed that the manufacturing limitations of the SOIMUMPs process had led to flexible leg geometries significantly deviated from the design. Hence, a larger triangular etching area will be implemented onto the future design in order to accommodate the manufacturing tolerances of the flexible legs. To prevent the microparts from shifting during the tether breaking process, the design of the parallel microgrippers will be revised to provide a higher microgripper grasping force. For instance, a different jaw geometry for the microgripper or a strong retraction force from the microgripper compliant beams may help restrain the microparts from these minute vertical or horizontal movements causing small angular misalignment of the microparts.

In this work, the exact tilting angle of the microparts during the lateral releasing schemes was not evaluated experimentally. In many microassembly operations, this tilting angle may pose assembly issues and lead to failure in the micro-devices. Hence, in the future, the microparts would be inspected under the SEM or the stereomicroscope to evaluate the tilting angle.

References

[1] Peterson K 2005 A new age for MEMS *Proc. 13th Int. Conf. on Solid-State Sensors, Actuators and Microsystems* vol 1 pp 1–4

[2] Gad-el-Hak M 2006 *MEMS: Introduction and Fundamentals* (Boca Raton, FL: CRC/Taylor and Francis) pp 1–5 chapter 1

[3] Rebeiz G M and Muldavin J B 2001 RF MEMS switches and switch circuits *IEEE Microw. Mag.* **2** 59–71

[4] Beeby S, Ensell G, Kraft M and White N 2004 *MEMS Mechanical Sensors* (Norwood, MA: Artech House) p 7

[5] Smart Equipment Technology FC150 Automated Device Bonder Brochure (Saint Jeoire: SET) pp 1–2, available at http://www.set-sas.fr/file/fichetechniquefc150.pdf

[6] Aarts A A A, Neves H P, Puers R P and Van Hoof C 2008 An interconnect for out-of-plane assembled biomedical probe arrays *J. Micromech. Microeng.* **18** 064004

[7] Popa D, Murthy R, Mittal M, Sin J and Stephanou H 2005 M^3-mocular multi-scale assembly system for MEMS packaging *Proc. IEEE Int. Conf. on Intelligent Robots and Systems* pp 3172–7

[8] Das A N, Zhang P, Lee W H, Popa D and Stephanou H 2007 μ^3: multiscale, deterministic micro-nano assembly system for construction of on-wafer microrobots *Proc. IEEE Int. Conf. on Robotics and Automation* pp 461–6

[9] Nelson B J, Zhou Y and Vikramaditya B 1998 Sensor-based microassembly of hybrid MEMS devices *IEEE Control Syst. Mag.* **18** 35–45

[10] Dechev N, Basha M, Chaudhuri S K and Safavi-Naeini S 2006 Microassembly of 3D micro-mirrors as building elements for optical MEMS switching *Proc. SPIE* **6376** 63760C

[11] Saini R, Jandric Z, Tsui K and Udeshi T 2004 Assembled micro-electromechanical-systems microcolumn from a single layer silicon process *J. Vac. Sci. Technol.* **22** 3168–73

[12] Murthy R, Das A and Popa D O 2008 ARRIpede: an assembled micro crawler *Proc. IEEE Int. Conf. on Intelligent Robots and Systems* pp 833–6

[13] Lai K W C, Chung P S, Li M and Li W J 2004 Automated micro-assembly of surface MEMS mirror by centrifugal force *Proc. World Congress on Intelligent Control and Automation* pp 23–8

[14] Feddema J T and Christenson T R 1999 Parallel assembly of LIGA components tutorial on modeling and control of micro- and nano-manipulation *Proc. IEEE Int. Conf. on Robotics and Automation* pp 1–17

[15] Tsui K, Geisberger A A, Ellis E and Skidmore G D 2004 Micromachined end-effector and techniques for directed MEMS assembly *J. Micromech. Microeng.* **14** 542–9

[16] Dechev N, Cleghorn W L and Mills J K 2006 Development of a 6 DOF robotic micromanipulator for use in 3D MEMS microassembly *Proc. IEEE Int. Conf. on Robotics and Automation* pp 281–8

[17] Wang L, Mills J K and Cleghorn W L 2008 Automatic microassembly using visual servo control *IEEE Trans. Electron. Packag. Manuf.* **31** 316–25

[18] Miller K, Cowen A, Hames G and Hardy B 2004 *SOIMUMPs Design Handbook* Rev 4.0 (Research Triangle Park, NC: MEMScAP) pp 1–24, available at http://www.memscap.com/mumps/documents/SOIMUMPs.dr.v4.pdf

[19] Dechev N, Cleghorn W L and Mills J K 2005 Design of grasping interface for microgrippers and micro-parts used in the microassembly *Proc. Int. Conf. on Information Acquisition* pp 134–9

[20] Ivanova K *et al* 2006 Thermally driven microgripper as a tool for micro assembly *Microelectron. Eng.* **83** 1393–5

[21] Prasad R, Bohringer K F and MacDonald N C 1995 Design, fabrication and characterization of single crystal silicon latching snap fasteners for microassembly *Proc. ASME IMECE* pp 917–23

[22] Liu J, Fan L and DeVoe D L 2005 Microfabricated sequential-leaf time-delay mechanisms *J. Microelectromech. Syst.* **14** 1051–60

[23] Chu H K, Mills J K and Cleghorn W L 2009 Microgripper design for use in parallel microassembly processes *Proc. 2nd Microsystems and Nanoelectronics Research Conf.* pp 61–4

[24] Stark B 1999 *Material properties MEMS Reliability Assurance Guidelines for Space Applications* (Pasadena, CA: NASA) p 50, available at http://trs-new.jpl.nasa.gov/dspace/bitstream/2014/18901/1/99-9001.pdf

[25] Whitney D E 1982 Quasi-static assembly of compliantly supported rigid parts *J. Dyn. Syst. Meas. Control* **104** 65–77

[26] Yeo T T E, Ong S H, Jayasooriah and Sinniah R 1993 Autofocusing for tissue microscopy *Image Vis. Comput.* **11** 629–39

[27] Gierl C, Kondo T, Voos H, Kongprawechon W and Phoojaruenchanachai S 2007 Automatic focusing of a motorized photo slit lamp microscope *Proc. 29th Ann. Int. Conf. of the IEEE EMBS* pp 3078–81

[28] National Instruments 2003 *IMAQ Vision for LabVIEW User Manual*, available at http://www.ni.com/pdf/manuals/371007a.pdf

[29] Chu H K, Mills J K and Cleghorn W L 2010 Dynamic tracking of moving objects in microassembly through visual servoing *Proc. IEEE Int. Conf. on Mechatronics and Automation* pp 1738–43